

UNCLASSIFIED

LEVEL II

12

SECURITY CLASSIFICATION OF THIS PAGE (When Data Entered)

REPORT DOCUMENTATION PAGE READ INSTRUCTIONS BEFORE COMPLETING FORM

1. REPORT NUMBER: AFOSR-TR-80-1007
2. GRANT OR SUBMISSION NO.: AD-A091087
3. RECIPIENT'S CATALOG NUMBER: 12 39

4. TITLE (and Subtitle): ANALYSIS FOR COHERENT ANTI-STOKES RAMAN SPECTROSCOPY (CARS)
5. TYPE OF REPORT & PERIOD COVERED: Final; Jan. 1 to June 30, 1980
6. PERFORMING ORG. REPORT NUMBER:

7. AUTHOR(s): Herschel Weil
8. CONTRACT OR GRANT NUMBER(s): AFOSR-80-0106

9. PERFORMING ORGANIZATION NAME AND ADDRESS: The University of Michigan, Department of Electrical and Computer Eng., Ann Arbor, MI 48109
10. PROGRAM ELEMENT, PROJECT, TASK AREA & WORK UNIT NUMBERS: 61102F, 2301/A1

11. CONTROLLING OFFICE NAME AND ADDRESS: AFOSR/NP, Bolling AFB DC 20332
12. REPORT DATE: 11 Jun 80
13. NUMBER OF PAGES: 36

14. MONITORING AGENCY NAME & ADDRESS (if different from Controlling Office): Final rept. 1 Jan-30 Jun 80
15. SECURITY CLASS. (of this report): UNCLASSIFIED
15a. DECLASSIFICATION/DOWNGRADING SCHEDULE:

16. DISTRIBUTION STATEMENT (of this Report): Approved for public release; distribution unlimited.
17. DISTRIBUTION STATEMENT (of the abstract entered in Block 20, if different from Report): 14 017896-1-F

DTIC ELECTRIC
NOV 04 1980

18. SUPPLEMENTARY NOTES:

19. KEY WORDS (Continue on reverse side if necessary and identify by block number): Raman spectroscopy, CARS

20. ABSTRACT (Continue on reverse side if necessary and identify by block number): see next page

294200
UNCLASSIFIED

AD A091087

DDC FILE COPY

✓

ABSTRACT

Coupled differential equations have been formulated which model the generation of coherent anti-Stokes Raman radiation in molecular gases. The equations include not only the basic term which involves the coherent interaction of incident pump and idler (Stokes) waves to generate the anti-Stokes radiation, but also include additional terms which model other radiation and absorption processes, both stimulated and coherent, which occur simultaneously. These are important in determining saturation effects due to population depletion of the lowest energy level. Other effects have also been considered. These are a finite idler beam bandwidth (simultaneous excitation of more than one vibration frequency) a quasi-monochromatic idler beam slightly off the true Stokes frequency; laser pulse shape; modification of the result for different rotational levels.

A number of different computer codes have been developed to solve the equations at different levels of complexity. With them numerical investigation of the effects of various physical factors on saturation was carried out. Some of the results are presented graphically.

↑

Accession For	
NTIS GRA&I	<input type="checkbox"/>
DDC TAB	
Unannounced	
Justification _____	
By _____	
Distribution/	
Availability Codes	
Dist.	Avail and/or special
A	

AFOSR-TR- 80 - 1007

**ANALYSIS FOR COHERENT ANTI-STOKES RAMAN SPECTROSCOPY
(CARS)**

FINAL REPORT

1 January 1980 - 30 June 1980

June 1980

Grant No. AFOSR-80-0106

by

**Herschel Weil
Radiation Laboratory
The University of Michigan
Ann Arbor, Michigan 48109**

Prepared for:

**United States Air Force
Air Force Office of Scientific Research
Building 410
Bolling AFB, D.C. 20332**

**Approved for public release;
distribution unlimited.**

80 10 9 099

ANALYSIS FOR COHERENT ANTI-STOKES RAMAN SPECTROSCOPY
(CARS)

Abstract

Coupled differential equations have been formulated which model the generation of coherent anti-Stokes Raman radiation in molecular gases. The equations include not only the basic term which involves the coherent interaction of incident pump and idler (Stokes) waves to generate the anti-Stokes radiation, but also include additional terms which model other radiation and absorption processes, both stimulated and coherent, which occur simultaneously. These are important in determining saturation effects due to population depletion of the lowest energy level. Other effects have also been considered. These are a finite idler beam bandwidth (simultaneous excitation of more than one vibration frequency) a quasi-monochromatic idler beam slightly off the true Stokes frequency; laser pulse shape; modification of the result for different rotational levels.

A number of different computer codes have been developed to solve the equations at different levels of complexity. With them numerical investigation of the effects of various physical factors on saturation was carried out. Some of the results are presented graphically.

AIR FORCE OFFICE OF SCIENTIFIC RESEARCH (AFSC)
NOTICE OF TRANSMITTAL TO DDC
This technical report has been reviewed and is
approved for public release LAW AFR 190-12 (7b).
Distribution is unlimited.
A. D. BLOSE
Technical Information Officer

I. INTRODUCTION

Coherent anti-Stokes Raman Spectroscopy is a form of Raman spectroscopy which has developed with the advent of laser light. In it the medium--usually gas or liquid--is irradiated by two waves, the pump wave at frequency ω_p and a lower frequency wave, the idler wave, at ω_I . When their frequency difference matches a vibrational frequency ω_v characteristic of the molecule the idler wave is then at the Stokes frequency $\omega_s = \omega_p - \omega_v$. One result is coherent generation of a new wave at the anti-Stokes frequency $\omega_a = 2\omega_p - \omega_s = \omega_p + \omega_v$ provided the incident wave intensities are adequate to excite the third order nonlinear terms in the electric susceptibility of the gas. For collinear phase-matched beams the intensity or power per unit area, I_a , in the new wave is roughly proportional to the square of the incident pump intensity, I_p , times the incident Stokes intensity, I_s , and also is proportional to the square of the distance over which the phase matched interaction occurs. Thus a very intense anti-Stokes output can be generated, orders of magnitude greater than spontaneous Raman scattering. Furthermore, unlike spontaneous Raman scattering, it is directional so that all the anti-Stokes radiation can be readily collected. Because of these two properties as well as others the generation of CARS spectra offers a potentially very practical tool for the measurement of molecular species concentrations and temperature in gases. It is especially useful as a probe of combustion gases since these commonly contain many particulates which can so strongly scatter incident radiation and also, due to the laser heating, radiate themselves, they can cause relatively weak spontaneous Raman radiation to be lost in the particle generated "noise"

while the far stronger CARS scattering would not be. Even with no particles in the gas ordinary spontaneous Raman scattering is in fact much weaker than the Rayleigh scattering which arises from the gas molecules and there is also interference due to fluorescent radiation. Because of these considerations AFAPL is actively laying the groundwork for the use of CARS as an eventually routine diagnostic tool for combustion systems.^{1,2,3}

The relation between measured CARS spectra for gases and the usually desired quantities; molecular species concentrations and temperature must be made on the basis of theory taking into account both the particular experimental setup as well as modification of the internal molecular structure of the constituent molecules by the applied and internally generated electromagnetic fields. The theory also requires a combination of quantum mechanical considerations regarding the populations of the molecular vibrational and rotational energy levels and transitions between them and classical wave propagation. The latter accounts for the coherency in the interactions between the various waves which is a fundamental part of the CARS generation of the anti-Stokes wave.

By limiting the theory to the most essential physical factors which explain CARS a convenient basic analytical formula for the CARS intensity results which gives the proportionalities discussed above. While the formula has clearly been of great value in a general understanding of CARS it is inadequate for the accurate quantitative prediction of the CARS spectra under certain conditions. In particular, it is quite inadequate to predict saturation effects which occur as

I_p , I_s or both are increased. It is also inadequate to treat the case when the idler beam is not quasi-monochromatic but contributes to excitation of more than one vibrational line simultaneously. For saturation effects to be accurately predicted requires the inclusion of stimulated generation and absorption of the pump, idler and anti-Stokes waves as well as stimulated and coherent generation of the second order Stokes wave at the frequency $\omega_x = \omega_p - 2\omega_v = 2\omega_s - \omega_p$ "symmetrical" with the anti-Stokes frequency $2\omega_p - \omega_s$. This is the so-called "scissors" CSRS process. All these processes occur simultaneously with CARS.

In this report we outline the derivation of the governing differential equations very concisely since much of it directly parallels results already in the literature except that here some additional physical processes and refinements are included. Aspects of the numerical integration problem are discussed and numerical results presented with emphasis on effects occurring due to depletion of the population of the lowest vibrational energy level.

II. DERIVATION OF EQUATIONS TO MODEL CARS

A. Physical Basis for CARS

To describe the generation of CARS spectra we consider the vibrational energy level diagram, Figure 1, showing the potential energy

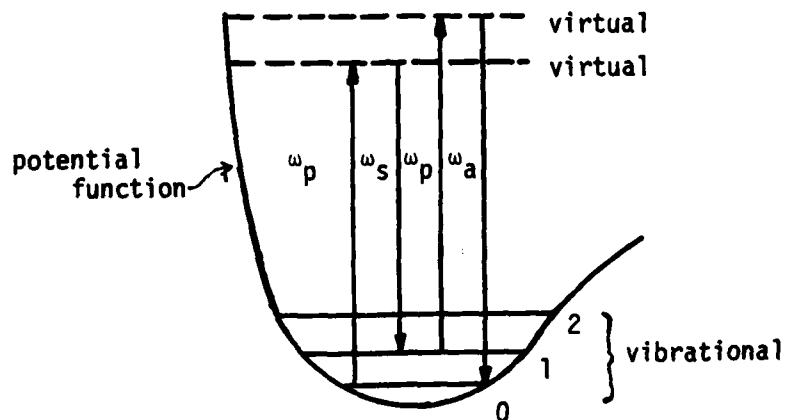


Figure 1. CARS

function and the ground state and two higher vibrational energy levels for a diatomic molecule. When a gas of such molecules is pumped by intense laser radiation of circular frequency ω_p , the set of simultaneous coherent photon-molecule interactions illustrated in Fig. 1 can be set up by coherent interaction of the electromagnetic and vibrational waves; absorption of two pump photons, emission of a photon at $\omega_s = \omega_p - \omega_1$, the Stokes frequency and at $\omega_a = 2\omega_p - \omega_s = \omega_p + \omega_1$,

the anti-Stokes frequency. If the gas is also irradiated by an external source at the Stokes frequency the emission of anti-Stokes radiation is greatly increased, primarily because the nonlinear term proportional to $|E_p|^2 E_s^*$ in the induced polarization of the gas is enhanced. In the CARS experimental systems at AFAPL, the gas is irradiated by collinear pump and idler laser beams of the same polarization. These are focussed into a small region in the gas so as to obtain a high resolution as well as a high intensity. In the focal region the beams "neck down" to a short cylindrical region in which they may be considered to have plane phase fronts. These conditions will be assumed in what follows.

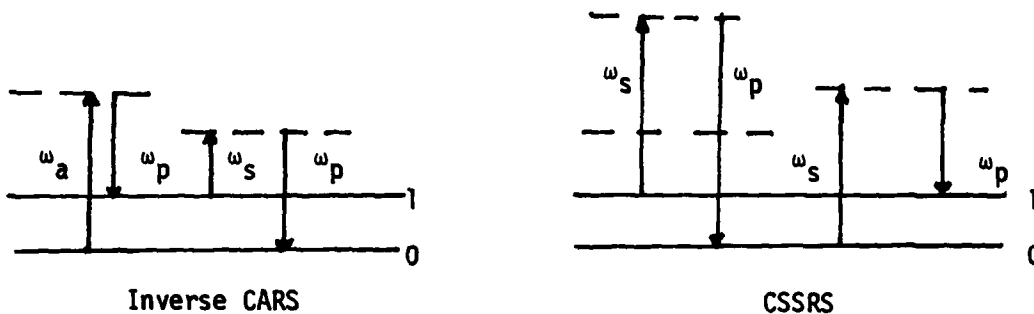
Along with CARS there are other coherent Raman processes which take place; inverse CARS and coherent secondary Stokes Raman (leading to CSSRS spectroscopy) and its inverse. These are illustrated by the diagram in Fig. 2 where it is seen that the CSSRS frequency $\omega_x = 2\omega_s - \omega_p = \omega_p - 2\omega_v$. There are also stimulated emissions which occur independently of one another and do not combine coherently as in CARS. These are shown in Fig. 3.

These processes are all induced by the lowest order electric field dependent--hence nonlinear--term in the susceptibility of the gas. In this point of view the induced molecular polarization may be written in terms of the electric field susceptibility tensors $\chi^{(1)}$ and $\chi^{(3)}$ as

$$P_i(t) = \chi_{i\alpha}^{(1)} E_\alpha(t) + \chi_{i\alpha\beta\gamma}^{(3)} E_\alpha E_\beta E_\gamma \quad (1)$$

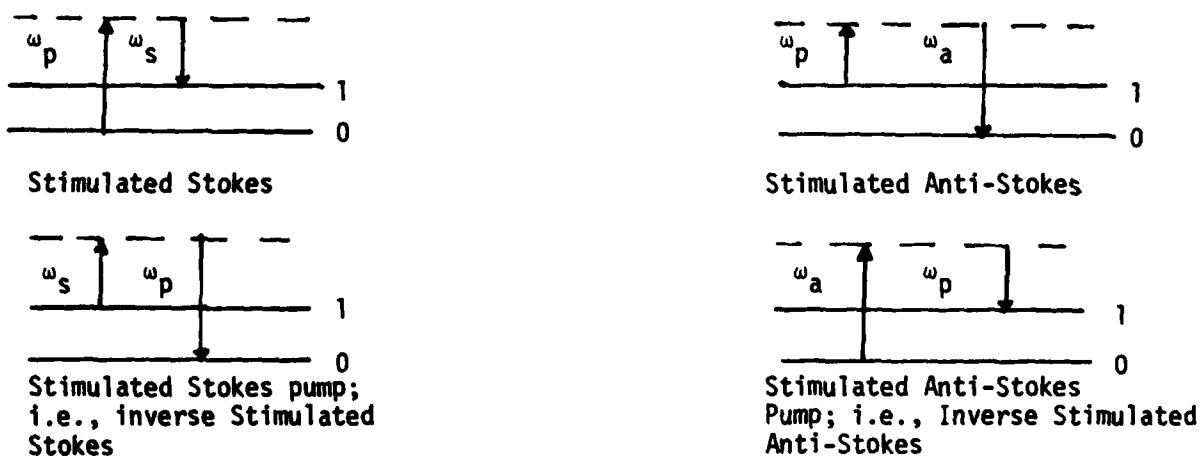
or as

$$\underline{P}(t) = \underline{P}^{(1)}(t) + \underline{P}^{(3)}(t) \quad (2)$$



Note: the populations of the vibrational level (1) and ground level (0) do not change because of these processes.

Figure 2. Coherent Raman Processes.



Note: the populations of the vibrational level and ground levels change as each process proceeds.

Figure 3. Stimulated Raman Scattering.

The vector \underline{E} is made of the sum of pump, idler, secondary Stokes and anti-Stokes components all with the same direction of propagation and the same linear wave polarization.

The stimulated processes alter the populations of the ground and energy levels. Furthermore, while all the processes shown in Figs. 1 through 3 involve only levels 0 and 1 the effect on the population of the additional process shown in Fig. 4.

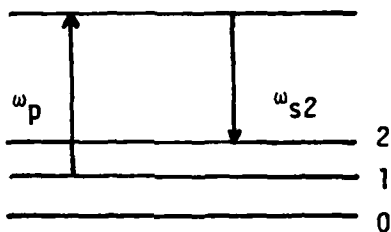


Figure 4. Stimulated Raman Scattering Involving Third Vibrational Level.

This difference Stokes frequency, $\omega_{s2} = \omega_p - (\omega_2 - \omega_1)$ differs from the Stokes frequency $\omega_s = \omega_p - \omega_1$ by a small percentage only. The difference is due to the lack of symmetry of the potential function as explained in Herzberg.⁴ Hence both processes will be stimulated by an incoming idler beam of even small bandwidth. For the equations to be presented in the following section we will ignore the process in Fig. 4. It will be considered again in Section D.

B. Two-Level Equations

The incident waves are assumed to be quasi-monochromatic collinear waves with the same wave polarization. Then the incident CARS and stimulated waves will also be collinear and with the same polarization as the incident waves. Accordingly, the total electric field may be written as a scalar sum

$$E(x,t) = \sum_{\alpha=1}^4 \left[A_{\alpha}(x,t) \exp(-i\omega_{\alpha}t + ik_{\alpha}x) + cc \right], \quad (3)$$

where α_1 stands for pump (p), α_2 for idler (I), α_3 for anti-Stokes (a), α_4 for secondary Stokes (X), and cc means complex conjugate. If the idler frequency is not the true Stokes frequency $\omega_I \neq \omega_S = \omega_p - \omega_1$ then by ω_a and ω_x in the following we will mean, respectively, $2\omega_p - \omega_I$ and $2\omega_I - \omega_p$. This is done to avoid additional notation such as possibly ω_{aI} and ω_{xI} . We are including the possibility of $\omega_I \neq \omega_S$ to be able to evaluate the rate of drop off in the anti-Stokes field with small deviations from the ideal resonant condition $\omega_I = \omega_S$.

Substitution of Eq. (2) into Maxwell's equations and elimination of the magnetic field in the usual way leads to the wave equations

$$\frac{\partial^2 E}{\partial x^2} - \frac{n^2}{c^2} \frac{\partial^2 E}{\partial t^2} = \frac{4\pi}{c^2} \frac{\partial^2}{\partial t^2} p^{(3)}(x,t) \quad (4)$$

When Eqs. (3) and (1) are substituted in (4) and terms with a common frequency equated one finds a set of equations for the E_{α}

$$\frac{\partial^2 E_\alpha}{\partial x^2} + \frac{n^2 \omega^2}{c^2} E_\alpha = - \frac{4\pi}{c^2} \omega_\alpha^2 p_\alpha^{(3)}(x) \quad (5)$$

These equations for the E_α are coupled through the $p_\alpha^{(3)}(x)$; these are terms which require expressions for the $\chi_{i\alpha\beta\gamma}^{(3)}$ of Eq. (1) before they can be expressed explicitly. For proper quantum mechanical derivations of the third order susceptibilities we refer to Druet and Taran⁵ where it is shown that, for the waves with frequencies $\omega_p - \omega_{\alpha'}$, they take the form for stimulated scattering

$$\chi_{p\alpha}^{(3)} = \frac{N}{h} \frac{(N_{v''} - N_{v'})c^4}{\omega_s^4} \left(\frac{d\sigma}{d\Omega} \right)_{v'} \frac{1}{(\omega_{v''} - \omega_{v'}) - \omega_p + \omega_{\alpha'} + i\Gamma_{v''v'}} \quad (6)$$

or its conjugate for coherent scattering. Here α' represents Stokes, anti-Stokes or secondary Stokes and the transition in question is between vibrational levels v' and $v'' = v' + 1$. $N_{v''}$ and $N_{v'}$ are their respective population densities and $N = N_{v''} + N_{v'}$. $(d\sigma/d\Omega)$ is the spontaneous Raman scattering cross section.*

*The cross section used here is ω_s/ω_p times the cross section in Druet and Taran.⁵

In addition to the above considerations we use

$$\frac{\partial^2 E_\alpha}{\partial x^2} = \frac{\partial^2 A_\alpha \exp(-i\omega t + k_\alpha x)}{\partial x^2} = \frac{\partial^2 E_\alpha}{\partial x^2} + 2ik \frac{\partial E_\alpha}{\partial x} - k^2 E_\alpha \quad (7)$$

The explicit equations which result from the substitution of the forms like Eq. (6) into (1) and (5) and then equating coefficients of $e^{-i\omega t}$ are

$$\frac{\partial A_\alpha}{\partial x} = F_\alpha \quad (8)$$

$$\frac{\partial F_\alpha}{\partial x} = -4\pi\nu_\alpha i(F_\alpha - if_\alpha) \quad (9)$$

where α represents pump, idler, anti-Stokes and secondary Stokes, i.e., p, I, a and X, respectively, and:

$$\nu_\alpha = \text{inverse wavelength (cm)}$$

$$f_a = 12\pi^2\nu_a [x_{pI} A_I^* A_p^2 e^{ix\Delta k} + x_{ap} A_a |A_p|^2 + x_{IX} A_X^* A_I A_p e^{ix\delta k}] \quad (10)$$

$$f_X = 12\pi^2\nu_X [x_{pI}^* A_p^* A_I^2 e^{ixDk} + 4ix_{ap}^* A_p A_a^* A_I e^{ix\delta k} + x_{IX}^* A_X |A_I|^2] \quad (11)$$

$$f_I = 12\pi^2\nu_I [x_{ap}^* A_a^* A_p^2 e^{ix\Delta k} + (x_{pI}^* |A_p|^2 A_I + x_{IX} |A_X|^2 A_I)] \quad (12)$$

$$f_p = 12\pi^2\nu_p [(x_{pI} |A_I|^2 + x_{ap} |A_a|^2) A_p + (x_{pI}^* + x_{ap}) A_I A_a A_p^* e^{-ix\Delta k} + x_{IX} A_X^* A_I^2 e^{ixDk}] \quad (13)$$

Here

$$\Delta k = 2k_p - k_I - k_a$$

$$\delta k = k_p + k_I - k_X - k_a$$

$$Dk = 2k_I - k_p - k_X \quad (14)$$

Clearly, this set of equations could be cut almost in half and hence be simpler and much cheaper to solve numerically if the second derivatives in A_α , the $\partial F_\alpha / \partial x$ terms governed by Eq. (9) were negligible. Furthermore, boundary conditions on the F_α are not normally available from the experimental data so to integrate the present set one has to estimate the boundary conditions by an analytic iterative procedure. This is given in the Appendix.

From physical considerations one expects that the terms $\partial F_\alpha / \partial x$ will have almost no influence on the results and we have verified this in a few numerical runs. In all other work we assumed that $\partial F_\alpha / \partial x = 0$.

For efficient computing separate codes based on setting (9) to zero

$$F_\alpha = if_\alpha \quad (15)$$

were used when the $\partial^2 A_\alpha / \partial x^2$ terms were to be neglected.

In these equations we must also bear in mind that the population difference ($N_0 - N_1$) is variable in time because of the stimulated Raman induced population changes indicated in Figure 2. In addition there is decay from any value $N_1 > N_{10}$ to the value N_{10} where N_{10} is the thermal equilibrium value. This is due to collisional interactions in which the vibrational energy of the molecules is converted to vibrational energy. This takes place with a relaxation time which is characteristic of the molecule in question as well as the other molecules in the gas, the pressure and temperatures.

To derive a differential equation for the time variation of $N_0 - N_1$ we consider that the photon density n in the incoming idler (Stokes) beam changes to $n + (\partial n/\partial x)dx$ in traversing a gas sample of length dx . The intensity of the incoming beam; i.e., the time averaged Poynting flux, is

$$I_I = \frac{c}{2\pi} A_S A_S^* = n \hbar \omega_S / (2\pi) \quad (16)$$

so that

$$\frac{\partial n}{\partial x} = \frac{c}{\hbar \omega_I} \left(A_I \frac{\partial A_I^*}{\partial x} + A_I^* \frac{\partial A_I}{\partial x} \right) \quad (17)$$

We have

$$\frac{\partial A_I}{\partial x} = i f_I |SRS \quad (18)$$

where f_I is given by the stimulated Raman terms in Eq. (12);

$$f_I|_{SR} = 12\pi^2 \nu_I \{x_{PI}^* A_I |A_P|^2 + x_{IX} A_I |A_X|^2\} \quad (19)$$

Then we find that

$$\frac{\partial \Delta}{\partial t} + \frac{\Delta}{\tau} + \frac{24\pi}{hN} |A_I|^2 (x_{PI}^* |A_P|^2 + x_{IX} |A_X|^2) = \frac{\Delta_0}{\tau} \quad (20)$$

and Δ_0 is the value of Δ at thermal equilibrium, τ is the relaxation time for transition from levels $v = 1$ to $v = 0$. The subscript i indicates imaginary part. Here Δ is the quantity

$$\Delta = \frac{N_1 - N_0}{N} \equiv \frac{N_1 - N_0}{N_1 + N_0} \quad (21)$$

To find N_V we use the Maxwellian distribution

$$N_V = N e^{-E_V/kT} / \sum_v e^{-E_V/kT} \quad (22)$$

where

$$E_V = hc[\omega_e(v + 1/2) - \omega_e x_e (v + 1/2)] \quad (23)$$

The quantities ω_e and $\omega_e x_e$ are available in Herzberg[†] for all diatomic molecules.

C. Simple CARS Formula

The dominant term in the generation of the anti-Stokes wave is the first term on the right-hand side of Eq. (10). This represents the coherent (CARS) process. To the extent that variation of A_I and A_P and $N_{\nu''} - N_{\nu'}$, (which enters into χ_{PI} as shown in Eq. (6)) and the other terms on the right-hand side in the equation can be ignored one then has, on integrating over $0 < x < L$

$$A_a = -12\pi^2 \nu_a \chi_{PI} A_I^* A_P^2 e^{i\Delta k} \frac{\sin \frac{L}{2} \Delta k}{\frac{L}{2} \Delta k} L \quad (24)$$

Using

$$I_a = \frac{c}{2\pi} A_a A_a^*$$

we get

$$I_a = \left(\frac{2\pi}{c} \right)^2 (12\pi^2 \nu_a \chi_{PI})^2 I_I I_P^2 \left(\frac{\sin \frac{L}{2} \Delta k}{\frac{L}{2} \Delta k} \right)^2 L^2 \quad (25)$$

One purpose of this investigation is to check how good a result (25) gives as one enters parameter ranges where the assumptions are not really valid.

D. Three-Level Equations

In this case $\nu = 0, 1$ and 2 . Vibrational transitions directly between levels 0 and 2 are forbidden; their probability is so low we need only consider the 01 and 12 transitions. Then introducing the two idler waves I_1 and I_2 of slightly differing frequencies equal to

or near to ω_s and ω_{s_2} where $\omega_{s_1} = \omega_p - \omega_1$, $\omega_{s_2} = \omega_p - (\omega_2 - \omega_1)$ we are led to two anti-Stokes waves $\omega_{a_1} = 2\omega_p - \omega_{I_2}$ and $\omega_{a_2} = 2\omega_p - \omega_{I_1}$. As in the earlier work the ω_{a_j} are not the "true" quantities $\omega_p + \omega_1$ and $\omega_p + (\omega_2 - \omega_1)$ unless $\omega_{s_1} = \omega_{I_1}$, $\omega_{s_2} = \omega_{I_2}$. We consider the two incident fields E_{I_1} and E_{I_2} although in physical practice there will likely be only one idler beam. The equations as written below can model this situation whether the beam is purely monochromatic or has a bandwidth sufficient to cover ω_{s_1} and ω_{s_2} .

The equations for the f_α are now found by replacing all the α subscripts by α_j , $j = 1$ or 2 except for subscript $\alpha = p$. The Δk , δk and Dk must likewise be subscripted 1 and 2. Thus, for example,

$$f_{I_j} = 12\pi^2 v_{I_j} \left[x_{a_j p}^* A_{a_j}^* A_p^2 e^{ix\Delta k_j} + x_{p I_j} |A_p|^2 A_{I_j} + x_{I_j} x_j |A_x|^2 A_{I_j} \right] \quad (22)$$

and similarly for f_{a_j} and f_{x_j} . On the other hand the Eq. (13) for f_p is replaced by just one equation,

$$f_p = 12\pi^2 v_p \sum_{j=1}^2 \left[(x_{p I_j} |A_{I_j}|^2 + x_{a_j p} |A_{a_j}|^2) A_p + (x_{p I_j} + x_{a_j p}) A_{I_j} A_{a_j} A_p^* e^{-ix\Delta k_j} + x_{I_j} x_j A_x^* A_{I_j}^2 e^{ixDk_j} \right] \quad (23)$$

We now have to obtain, for use in the $\chi_{\alpha\beta j}$, both

$$\Delta = \frac{N_0 - N_1}{N} \quad \text{and} \quad \Delta_{12} = \frac{N_2 - N_1}{N} \quad (24)$$

By a derivation directly analogous to that used for Eq. (16) but involving the stimulated Raman processes of both figures 3 and 4 we can obtain the appropriate equations. In terms of *

$$\Delta_1 \equiv \Delta \quad \text{and} \quad \Delta_2 = (N_2 - N_0)/N \quad (25)$$

$$\begin{aligned} \frac{\partial \Delta_1}{\partial t} = & -\frac{12\pi}{h N} |A_p|^2 (2|A_{s_1}|^2 \chi_{1i} + |A_{s_2}|^2 \chi_{2i}) \\ & + \frac{1}{3} \left(\frac{1}{\tau_{20}} - \frac{1}{\tau_{21}} - \frac{4}{\tau_{10}} \right) (\Delta_1 - \Delta_{10}) \\ & + \frac{2}{3} \left(\frac{1}{\tau_{21}} - \frac{1}{\tau_{20}} + \frac{1}{\tau_{10}} \right) (\Delta_2 - \Delta_{20}) \end{aligned} \quad (26)$$

$$\begin{aligned} \frac{\partial \Delta_2}{\partial t} = & \frac{12\pi}{h N} |E_p|^2 (|A_{s_1}|^2 \chi_{1i} + |A_{s_2}|^2 \chi_{2i}) \\ & + \frac{1}{3} \left(\frac{2}{\tau_{20}} + \frac{1}{\tau_{21}} - \frac{2}{\tau_{10}} \right) (\Delta_1 - \Delta_{10}) \\ & + \frac{1}{3} \left(\frac{1}{\tau_{10}} - \frac{4}{\tau_{20}} - \frac{2}{\tau_{21}} \right) (\Delta_2 - \Delta_{20}) \end{aligned} \quad (27)$$

*The equations in terms of Δ_1 and Δ_2 are much better suited for numerical integration than equations in terms of Δ and Δ_{12} or in terms of N_1 and N_2 . This is because the rates of change of Δ_1 and Δ_2 are relatively slow while this is not true for N_2 and Δ_{12} near $t=0$.

D. Rotational Levels

The rotational energy levels, $E_{v,j}$, associated with each vibration level v have so far been ignored. If we limit ourselves to the Q branch transitions between vibrational states there is no change in the J value. For this case the previous equations are readily generalized so that they apply to a given rotational level J . Then one replaces formula (18) by the equilibrium values appropriate to the J th levels:

$$N_{v,J_0} = \frac{N(2J + 1)g_n e^{-(E_v + E_J)/(kT)}}{\sum_v e^{-E_v/kT} \frac{G_n kT}{(2\pi B \hbar c)}} \quad (28)$$

where E_v is given still by (19), $\hbar = h/(2\pi)$,

$$E_J = B \hbar c J(J + 1)/kT \quad (29)$$

and g_n and G_n are constants characteristic of the molecules in question. (see Herzberg⁶).

E. Measured Quantity-Energy

The main physical quantity which is measured experimentally is the anti-Stokes energy or power per unit area incident on a receptor surface at the end of the sample, integrated over the pulse time and the detector surface area. We are assuming uniform plane waves so the area integration is trivial. Hence the quantity we shall compute to model the experiment will be energy/area \mathcal{E}_a

$$\mathcal{E}_a^{(t)} = \frac{c}{2\pi} \int_0^T E_a^2|_{x_m} dt \equiv \int_0^T I_a dt . \quad (30)$$

Similarly we can compute the CSSRS energy

$$\mathcal{E}_x^{(t)} = \frac{c}{2\pi} \int_0^T E_x^2|_{x_m} dt . \quad (31)$$

The E_a and E_x are evaluated at the end, x_m , of the sample volume which extends to the right from $x = 0$, where it is irradiated.

III. COMPUTATIONS

A. Computer Codes

The equation sets of the previous section were programmed in FORTRAN IV for computation. For simplicity and speed in the computations separate programs, CARSO through CARS5, were written for different cases.

<u>Code Name</u>	<u>Main Equations</u>	<u>Number of Energy Levels (including ground)</u>	<u>Is CSSRS Included?</u>	<u>Are second derivative terms included?</u>	<u>Integration Method</u>
CARSO	(15), (20)	2	no	no	RK
CARS2	(22)-(27)	3	no	no	RK
CARS3	(15), (20)	2	no	no	A,M and G
CARS4	(8), (9), (20)	2	no	yes	RK
CARS5	(15), (20)	2	yes	no	RK

Here RK stands for 4th order Runge-Kutta, AM for Adams-Moulton and G for Gear's method. Provision was made in CARSO to set individual terms equal to zero on the right. Also CARS5 was set up to compute either Gaussian or rectangular shaped pump and idler pulses whereas the other codes are limited to rectangular.

Numerical comparisons between sample CARSO and CARS3 results showed no reason to favor AM or G over the RK method so RK was used for all the data presented.

The integration in space and time was organized to proceed between the discrete point mn shown in Figure 5 in a manner designed to minimize storage.

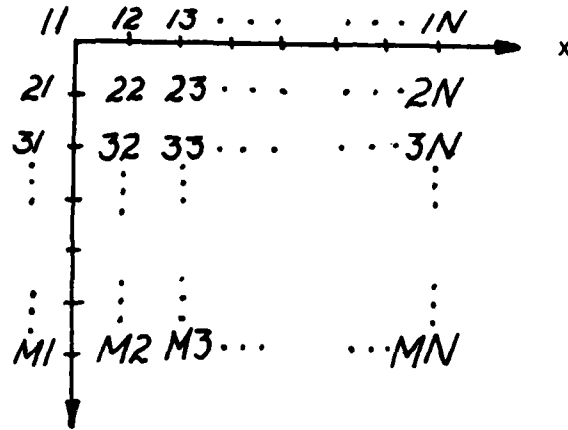


Fig. 5 Diagram to explain computation scheme.

To describe it let the symbolic statement $nm \rightarrow (n + 1)m$ mean to carry out the integrations of the A_α with respect to x between the points nm and $(n + 1)m$ while $nm \rightarrow n(m + 1)$ means to integrate the equations for Δ (or Δ_1 and Δ_2) with respect to time between nm and $n(m + 1)$. The integrations between the points were carried out using many further subdivisions whose size is adjustable automatically to fit pre-stated accuracy requirements. Distance x ranged from 0 to L while time was measured from 0 to T , with L and T chosen to correspond to values typical of experiments at AFAPL.

The computation was carried out using the following order and approximations:

11 → 21 using Δ_0 as initial value

11 → 12 using Δ_0 in computing χ 's

12 → 22 using Δ_0 as initial value

.....

.....

1(n - 1) 1 N using Δ_0 in computing χ 's

Then

21 → 31 using $\Delta(21)$ as initial value

21 → 22 using linear interpolation between (21) and (22) in computing χ 's

22 → 32 using $\Delta(22)$ as initial value

.....

.....

(M - 1)N MN using $\Delta((m - 1)N)$ as initial value.

Numerical comparison of simple CARSO and CARS4 results showed, as expected, almost no difference in the numerical results for the electric fields E_α or energies \mathcal{E}_α as computed with the second derivative terms or neglecting them. Keeping them however led to so tremendous an increase in computing time, that it was impractical from a cost standpoint to extend the computations as far in distance and time as would correspond to the CARS experimental work at WPAFB. In light of these results all subsequent work was done without second derivative terms.

Another comparison which was made was to run the same data using CARSO and CARS5. The results showed that there was practically no change in \mathcal{E}_a ; when CSSRS energy \mathcal{E}_x developed it was not at the expense of \mathcal{E}_a .

B. Presentation of the Results

\mathcal{E}_a for the various cases to be described has been plotted vs. $|A_p|^4 |A_I|^2 (= (2\pi/c)^3 I_p^2 I_I)$ on log paper.

If the simple CARS formula (25) were to hold then the computed curves would simply be straight lines at 45° to the axes. These lines would intercept the vertical axis at a height

$$\log \left(\frac{c}{2\pi} \right) (12\pi^2 v_a x_{pI})^2 \frac{\sin \left(\frac{L}{2} \Delta k \right)^2}{(L/2) \Delta k} L^2 T .$$

As $I_p^2 I_I$ increases the effect of the non CARS terms becomes non-negligible and with that goes the fact that changes in the energy population levels become important. The \mathcal{E}_a vs. $|E_p|^4 |E_I|^2$ plots bend below the straight line which results when these phenomena are neglected. This bending is the saturation effect referred to in the abstract and introduction.

To show how the bending of the \mathcal{E}_a curves is tied in with energy level depletion the corresponding curves of Δ or Δ_1 and Δ_2 vs $|E_p|^4 |E_I|^2$ are also plotted.

C. Data

Computations were made for N_2 . The corresponding constants needed to compute Δ_0 and the χ were taken from Hertzberg⁴. Relaxation times were taken from White and Millikan⁷. In CARS2 we need several relaxation times. We could find no such detailed data and have simply used a common τ value equal to the above. The actual data used

for the computational results presented in Section E is, (in Gaussian units)

$$\begin{aligned}v_V &= 0.2331 \text{ E04} \\v_I &= 0.1207 \text{ E05} \\v_p &= 0.1440 \text{ E05} \\d\sigma/d\Omega &= 0.3300 \text{ E-31}\end{aligned}$$

Notation:
(E04 \equiv 10^4 , etc.)

Case A:

$$\begin{aligned}p &= 0.7600 \text{ E} + 05 \\T &= 0.3000 \text{ E} + 04 \\\tau &= 0.400 \text{ E} - 06 \\(\Delta_0 &= 0.5080 \text{ E} + 00)\end{aligned}$$

Case B:

$$\begin{aligned}p &= 0.7600 \text{ E} + 05 \\T &= 0.1000 \text{ E} + 04 \\\tau &= 0.1000 \text{ E} - 04 \\(\Delta_0 &= 0.9328 \text{ E} + 00)\end{aligned}$$

These p , T and τ combinations are from the White and Millikan's empirical data and were chosen to illustrate the effects of varying τ . The Δ_0 values however also vary and their computed values are shown in parentheses.

D. Discussion of Results

Aside from the results discussed in the previous sections which do not lend themselves to graphical display we present a series of curves where $I_p^2 I_I$ is varied by changing I_p while keeping I_I fixed.

Figure 1 illustrates the buildup of \mathcal{E}_a with time by showing curves for $T = 10 \text{ ns}$ and $T = 20 \text{ ns}$ for each fixed level of pump and idler

irradiation. The curves show that once saturation due to increasing I_p becomes strong very little or no additional anti-Stokes power is delivered in the last half of a 20 ns rectangular pulse. While Δ drops closer to zero after 10 ns it has dropped so far from its initial value in 10 ns that very little further \mathcal{E}_a is generated. While examining the data in Figs. 1 through 5 note that the assumed temperature is quite high so that $\Delta_0 = 0.508$. CARS was used for curves A.1.

Figure 2 shows the effect of keeping the CARS term only in computing A_a assuming, when calculating χ , that A_p and A_I are constant but nevertheless allowing approximately for change in Δ by use of Eq. (20). The \mathcal{E}_a and Δ for this artificial case is labeled A.2 and is computed via CARS0. The Δ variation is only approximate because A_p and A_I were kept constant. Comparing A.2 to a correctly computed curve A.3 and to the 45° line (for CARS only and $\Delta \equiv \Delta_0$) gives an idea of how much of the saturation effect is due to Δ changing as opposed to how much is due to the neglect of the stimulated noncoherent generation of E_a .

Figure 3 illustrates the effect of using three vibrational levels instead of only two. The idler wave A_I in the three level case is taken in curves A.5 to be monochromatic so that $A_{I1} = 10^3$, $A_{I2} = 0$. For curves A.4 $A_{I1} = A_{I2} = 10^3$.

The two level corresponding curves are given by curve A.3. To interpret the curves for A.5 Δ_2 actually becomes negative by virtue of stimulated emissions from level 1. We have plotted $|\Delta_2|$ using a dashed curve for the portion of the curve which is plotted when Δ_2 is negative. In some instances we have also used the symbols \oplus and \ominus to indicate the sign of Δ_1 or Δ_2 .

is negative. We do not have enough data to draw in the curve in the missing intervening section corresponding to the $I_p^2 I_I$ range in which Δ_2 goes through zero.

We note that although the energy level populations are quite radically changed by the more complete analysis for curves A.4 and A.5 the \mathcal{E}_a curves of A.3 and A.5 differ only by a relatively small uniform translation for all $I_p^2 I_I$ values. The \mathcal{E}_a plotted for curve A.4 is the sum of $\mathcal{E}_{a1} + \mathcal{E}_{a2}$. It corresponds to the energy a receptor of uniform sensitivity across a frequency band covering ω_{a1} and ω_{a2} would receive.

Figure 4 presents several comparisons. Curves A.3 vs. A.6 exhibit the effect of Gaussian pulses (curve A.6) as compared to a rectangular pulse (A.3). The two pulses have the same duration and peak power so that the incident Gaussian pump and idler pulses deliver 81% as much energy as the rectangular pulses. 81% of the \mathcal{E}_a output for the rectangular pulse is shown as an additional curve in the figure.

Curves A.3 vs. A.9 exhibit the effect of achieving the same range of $I_p^2 I_I$ by multiplying I_I by 10 and dividing I_p accordingly by $\sqrt{10}$. The large difference in results indicates inaccuracy in the simple CARS formula.

In Figure 5 the curves A.3 vs. A.10 exhibit the effect of changing τ from $\tau = 0.4 \text{ E} - 06$ for (A.3) to $\tau = 0.1 \text{ E} - 06$ for A.10, keeping all other parameters constant (even though τ is a function of, for example, temperature). The difference in output is less than the accuracy with which the figures are drawn.

Curves A.3 vs. A.7 show the effect of decreasing the coherence length by setting $\Delta k = Dk = \delta k = 10.7$ for A.7 against setting $\Delta k = Dk = \delta k = 0$ for A.3.

Figure 6 depicts the direct analog of Figure 3 but carried out for the data of Case B as given above in Section C. In this case the excitation $A_{I1} = 10^3$, $A_{I2} = 0$ corresponds to curve B.3 and $A_{I1} = A_{I2} = 10^3$ to curve B.3. The two-level case is curve B.2.

APPENDIX

Boundary Conditions

To solve the equations (8) and (9) requires boundary conditions on A_α and $F_\alpha = (\partial A_\alpha / \partial x)$ at $x = 0$.

For the A_α we have A_p and A_I given nonzero values (determined by the experimental set-up) while A_a and $A_x = 0$. $A_a = 0$ assumes no anti-Stokes is generated in the gas outside the test region--or at least that it is negligible.

To obtain boundary conditions on the derivatives is more difficult in a sense since these are not normally specified or measured. We use the following approximate procedure. Referring to Eqs. (8) through (13), we first consider χ 's independent of x and $F_\alpha = if_\alpha$; i.e.,

$$\frac{\partial A_\alpha}{\partial x} = if_\alpha \quad . \quad (A.1)$$

Then

$$\left. \frac{\partial F_\alpha}{\partial x} \right|_{x=0} = \left. \frac{\partial^2 A_\alpha}{\partial x^2} \right|_{x=0} = \left. \frac{\partial F_\alpha}{\partial x} \right|_{x=0} \quad (A.2)$$

where, in evaluating $(\partial f_\alpha / \partial x)|_{x=0}$, we use the boundary conditions on A_α and the fact that $F_\alpha = if_\alpha$. The result is that the $(\partial F_\alpha / \partial x)|_{x=0}$ can be written explicitly as functions of $A_p(0,t)$ and $A_s(0,t)$. Then

$$F_{\alpha}|_{x=0} = i \left[\frac{1}{4\pi v_0} \frac{\partial F_{\alpha}}{\partial x} + f_{\alpha} \right]_{x=0} \quad (A.3)$$

These are the values used to start the solutions of (8) and (9).

Specifically, one has

$$\frac{\partial F_a}{\partial x} \Big|_0 = -12\pi^2 v_a x A_p^2 A_s \left\{ 12\pi^2 [2x v_p |A_s|^2 + (v_a x + v_s x^*) |A_p|^2] + \Delta k \right\} \Big|_{x=0}$$

$$\frac{\partial F_s}{\partial x} \Big|_0 \cong (12\pi^2)^2 v_s A_s |A_p|^2 x^* \left\{ v_a |A_p|^2 x^* - 2i |A_s|^2 v_p x_i - |A_p|^2 v_s x^* \right\} \Big|_{x=0}$$

$$\frac{\partial F_p}{\partial x} \Big|_0 \cong (12\pi^2)^2 x A_p |A_s|^2 v_p \left\{ 2 |A_p|^2 (i v_s x_i - v_a x_r) - v_p x |A_s|^2 \right\} \Big|_{x=0}$$

where $x = x_r + i x_i$ and CSSRS has been neglected.

REFERENCES

1. Gary L. Switzer, W. M. Roquemore, Royce P. Bradley, Paul W. Schreiber, Won B. Roh., "CARS Measurements in a Bluff-Body Stabilized Diffusion Flame", *Appl. Op.* 18, 1979, pp. 2343-2345.
2. Won B. Roh, Robert F. Weber, Paul W. Schreiber, "Linewidth Determination by Integrated Power Measurement of Coherent Anti-Stokes Raman Scattering", *Optics Comm.*, 27, 1978, pp. 142-146.
3. Won B. Roh, Paul W. Schreiber, "Pressure Dependence of Integrated CARS Power", *Appl. Optics*, 17, 1978, pp. 1418-1424.
4. Gerhard Herzberg, *Molecular Spectra and Molecular Structure*, D. Van Nostrand Co., NY (1950).
5. Sylvie Druet, Jean-Pierre Taran, "Coherent Anti-Stokes Raman Spectroscopy", in *Chemical and Biochemical Applications of Lasers IV*, C. Bradley Moore, ed; Academic Press, N.Y. (1979).
6. Gerhard Herzberg, "Infrared and Raman Spectra of Polyatomic Molecules", D. Van Nostrand Co., New York (1945).
7. Donald R. White and Roger C. Millikan, "Vibrational Relaxation in Air", *AIAA J1.*, 2 (1964), pp. 1844-1846.

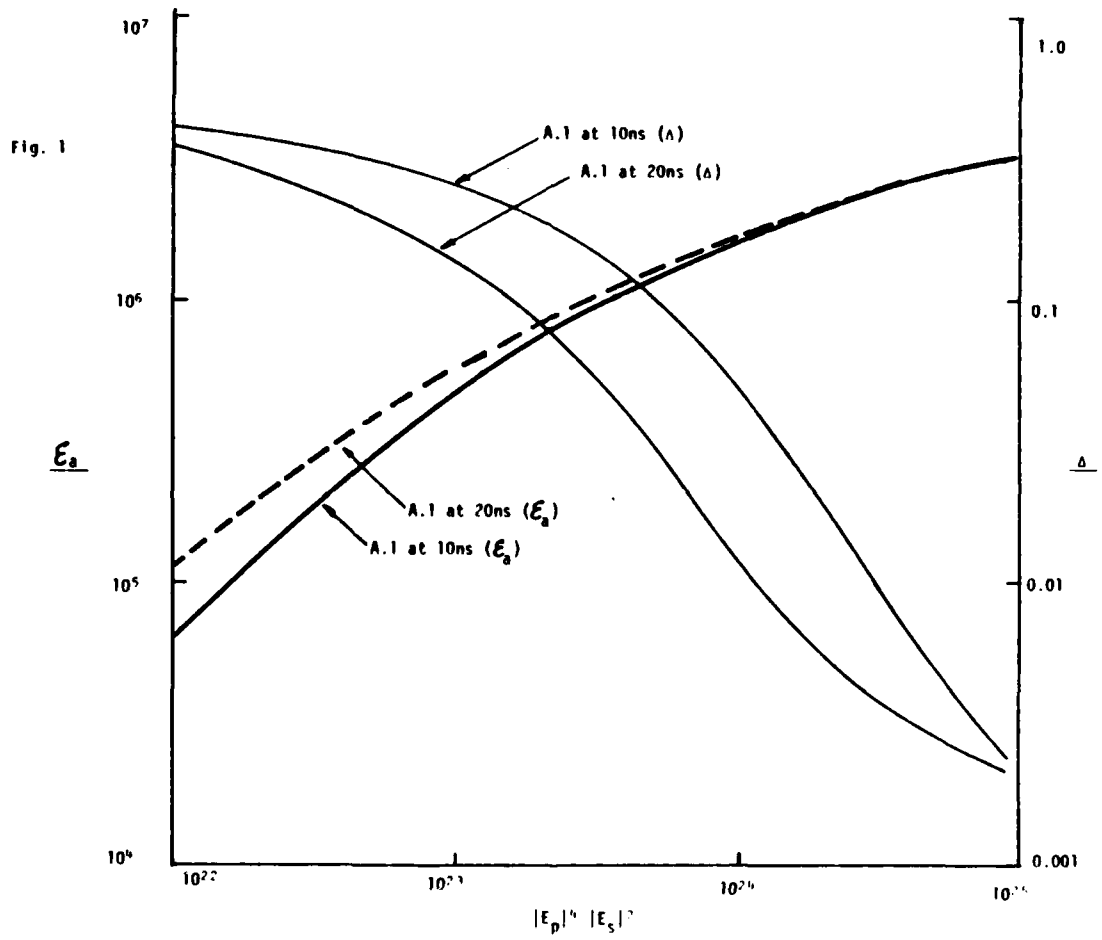


Fig. 1 CARS energy; effects of excitation duration.

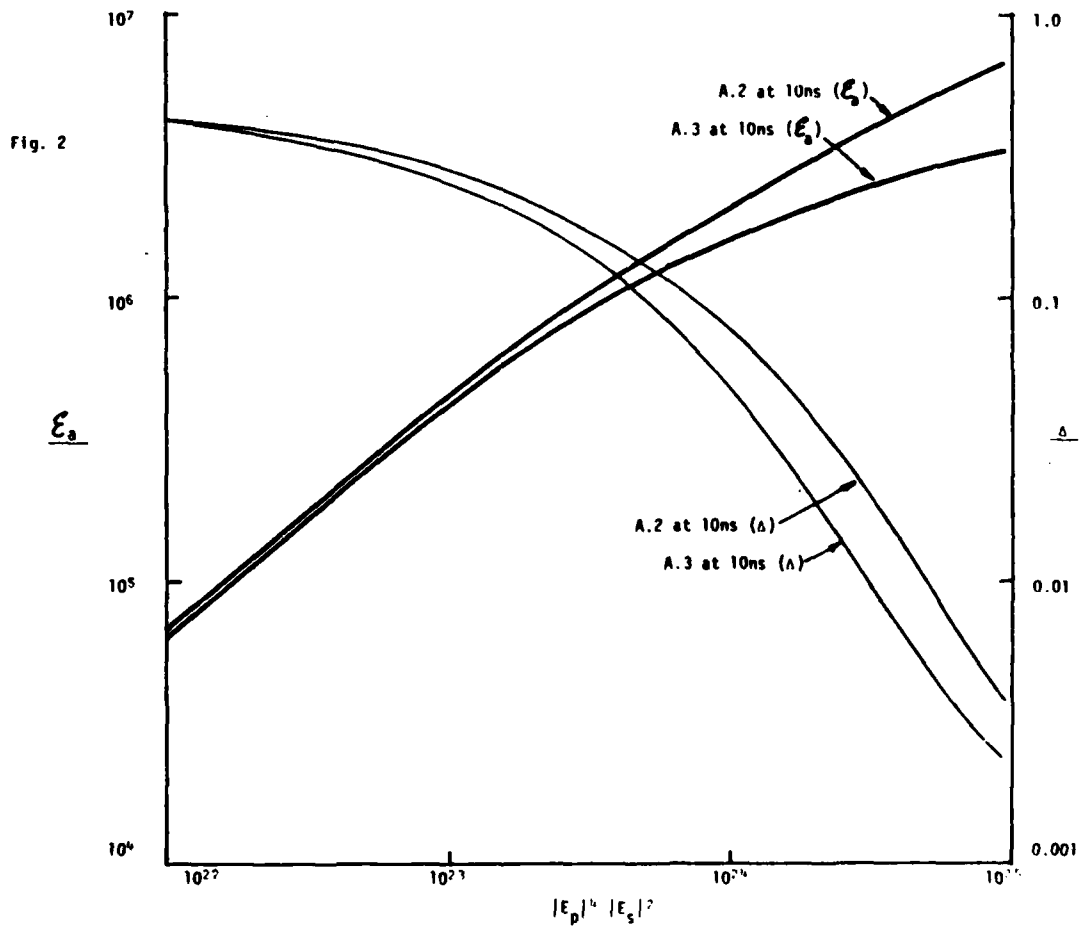


Fig. 2. CARS energy; effects of non-CARS terms.

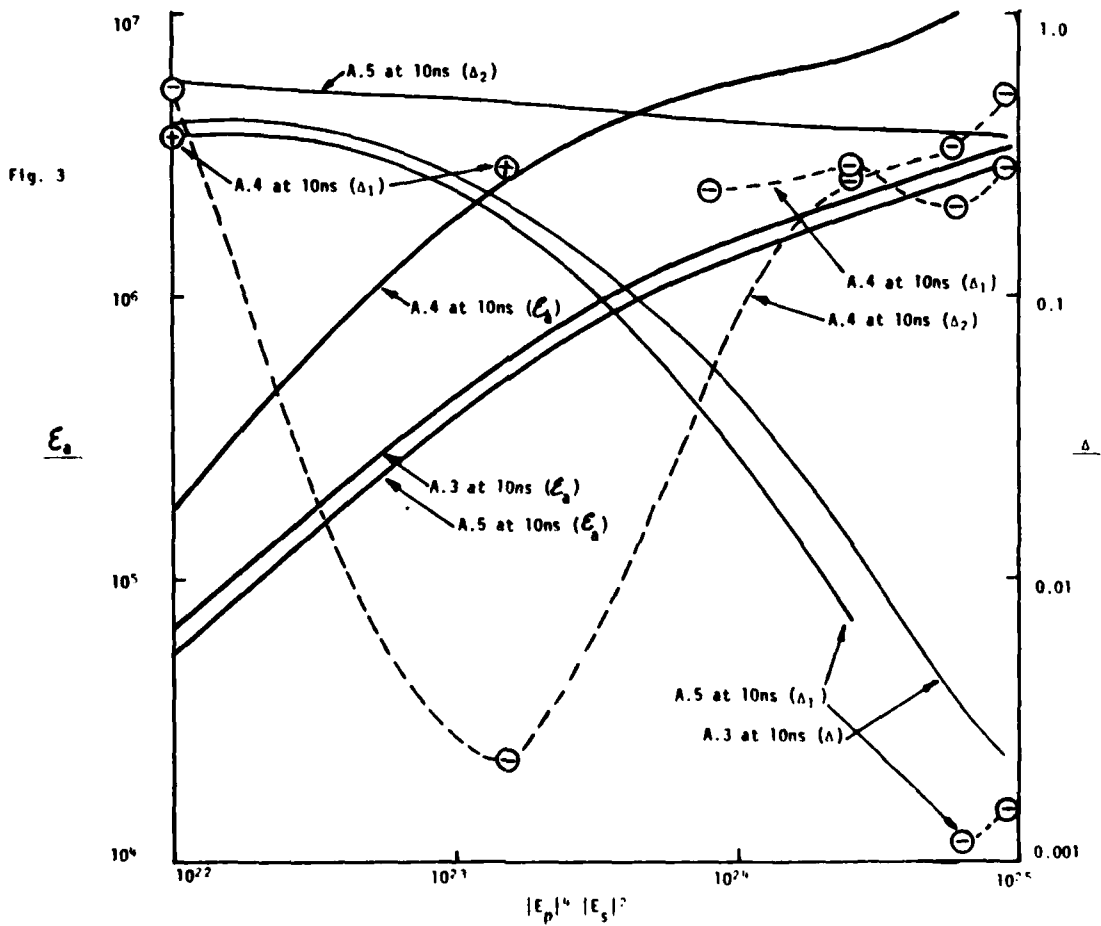


Fig. 3 CARS energy; effects of third vibrational level (Case A data).

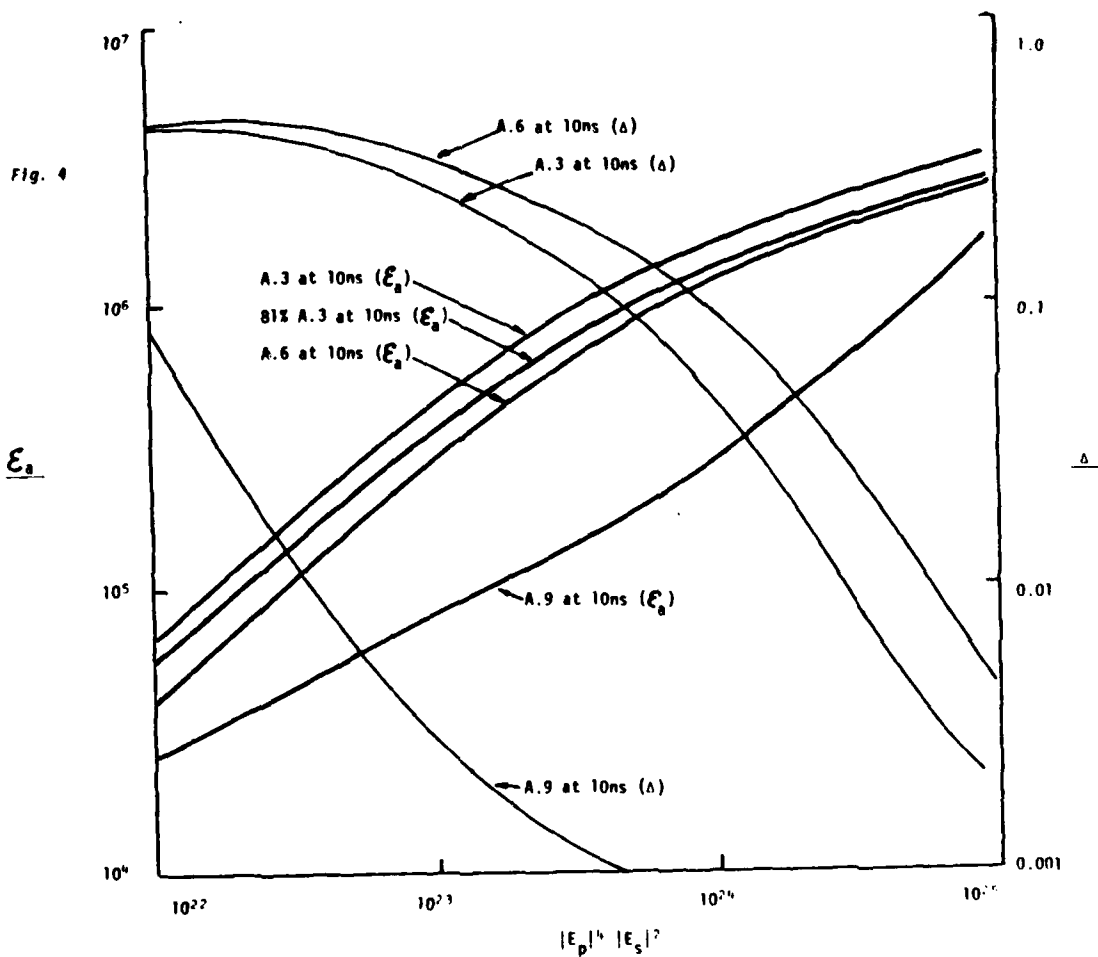


Fig. 4. CARS energy; effect of pulse shape; effect of changing I_p and I_s keeping $I_p^2 I_s$ fixed.

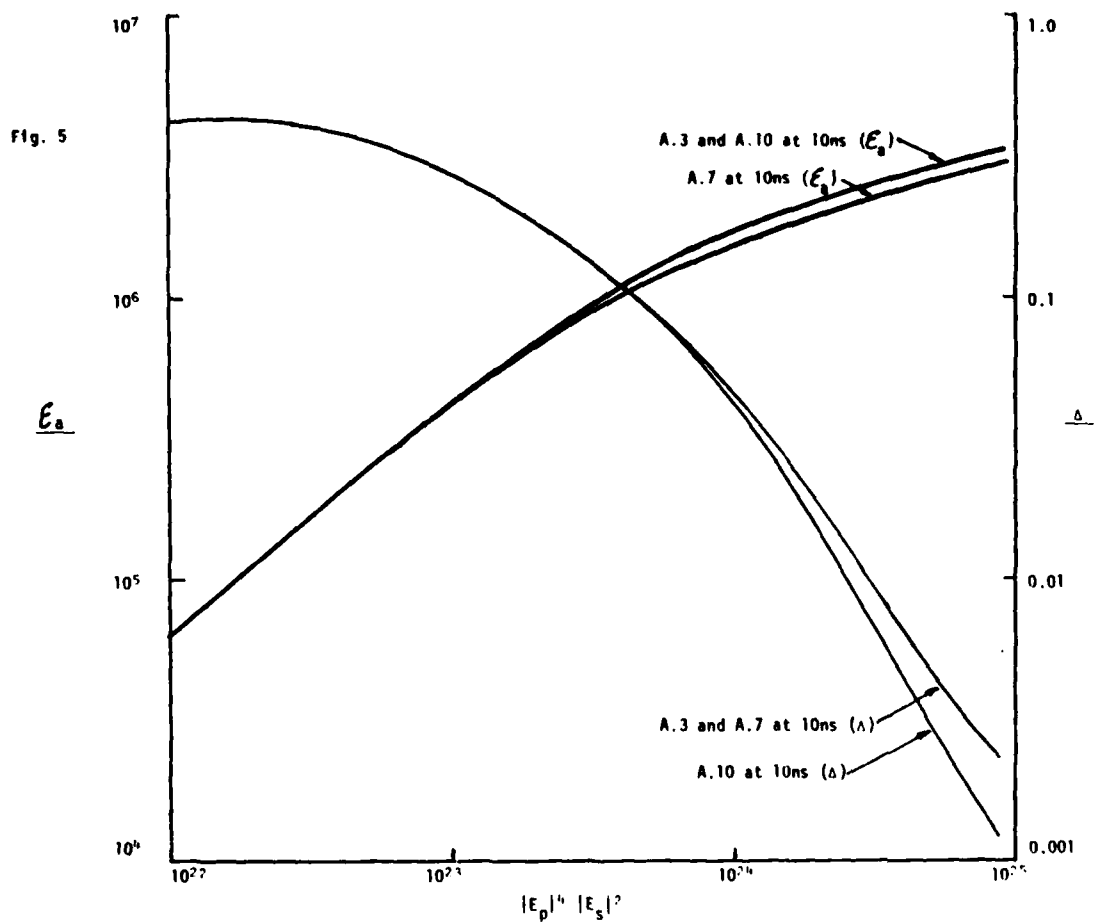


Fig. 5 CARS energy; effect of vibrational relaxation time.

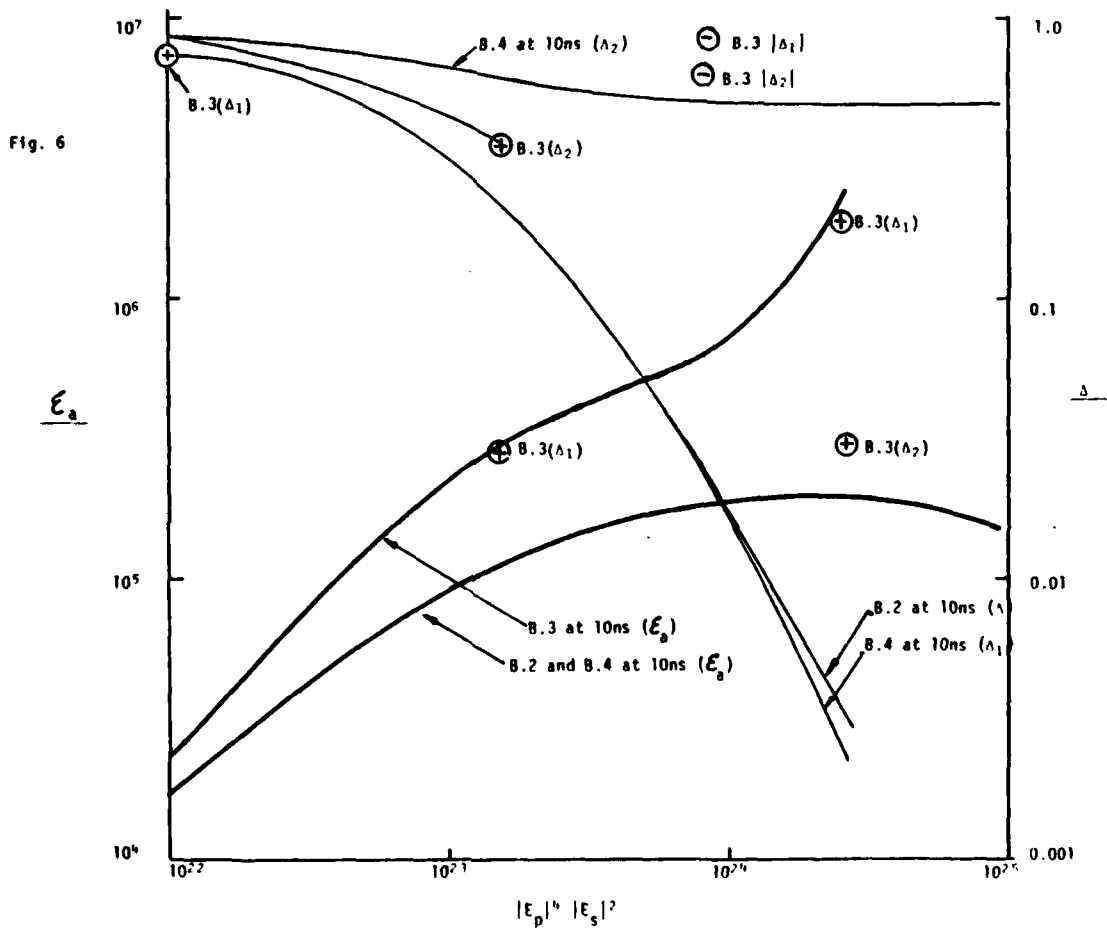


Fig. 6 CARS energy: effects of third vibrational level (Case B data).